Fully Coupled Rigid Internal Combustion Engine Dynamics and Vibration—Part II: Model-Experiment Comparisons

D. M. W. Hoffman[1]

D. R. Dowling

Department of Mechanical Engineering,
The University of Michigan,
Ann Arbor, MI 48109-2121

In internal combustion engine vibration modeling, it is typically assumed that the vibratory state of the engine does not influence the loads transmitted to the engine block from its moving internal components. This one-way-coupling assumption leads to energy conservation problems and does not account for Coriolis and gyroscopic interactions between the engine block and its rotating and reciprocating internal components. A new seven-degree-of-freedom engine vibration model has been developed that does not utilize this assumption and properly conserves energy. This paper presents time and frequency-domain comparisons of this model to experimental measurements made on an inline six-cylinder heavy-duty Diesel engine running at full load at peak-torque (1200 rpm) and rated (2100 rpm) speeds. The model successfully predicts the overall features of the engine's vibratory output with model-experiment correlation coefficients as high as 70 percent for vibration frequencies up through third engine order. The results are robust to variations in the model parameters. Predictions are less successful at the detail level and at higher frequencies because of uncertainties in the actual imperfections of the test engine, and because of the influence of unmodeled engine components.
[DOI: 10.1115/1.1370400]

1 Introduction

Fluctuating mechanical loads from piston-driven internal combustion (IC) engines are frequently the main source of low frequency vibration in transportation systems. Here, low frequencies are understood to lie in the range of the first few rotational orders of the running engine (up to eighth or tenth order). Even though standard isolation schemes provide excellent vibration isolation at higher frequencies, market forces still push for the reduction or elimination of low-frequency vibration in modern vehicles.

The amount of low-frequency vibration transmitted from an IC engine to a vehicle's structure is determined by the vibratory output of the engine, the location and resilience of the vibration-isolating engine mounts, and the characteristics of the vehicle's structure. Although large computationally expensive full-vehicle vibration models are possible, preliminary design work requires simple computationally efficient tools. Thus, simplified low degree-of-freedom models are required. More precisely, robust and accurate design and simulation models are needed to predict the vibratory output of mounted IC engines to minimize possible durability and customer-perceived quality problems associated with excessive vibration. Such models should execute quickly and require only relatively simple inputs so that optimization of engine parameters, engine mount locations, and isolator properties are possible.

Most engine vibration models rely on the assumption that the coupling forces between the engine's moving internal components and block are independent of the engine's vibratory motion ([1–5]). Thus the engine vibration problem is solved in two steps. First the moving internal components are simulated in a hypothetical engine that is rigid and stationary to predict coupling forces. Then, these coupling forces are applied to the resiliently supported engine block to determine its vibratory motion. This approach is approximate because it only allows for one-way coupling between the moving internal components and the block and does not account for Coriolis or gyroscopic coupling.

This paper presents low-frequency vibration comparisons between an actual running engine and the fully coupled seven degree-of-freedom engine dynamics and vibrations model described in a companion paper ([6]), hereafter referred to as Part I) and in Hoffman [7]. This fully coupled model (FCM) is based on rigid-body dynamics and does not rely on the one-way coupling assumption. The FCM properly includes all mechanical inter-actions between the rotating, reciprocating, and vibrating motions of the engine's crankshaft, flywheel, connecting rods, pistons, and block. Previous experimental work has shown that the rigid-body assumption is acceptable for low-frequency engine block vibrations ([8]).

The experimental engine for this study, an inline six-cylinder heavy-duty Diesel engine, was mounted on three-component load cells and run at peak-torque and rated-speed (power) operating points. Measurements from the load cells are compared to FCM simulations in both the time and frequency domains. Modal analysis and parameter optimization are used to determine the various inertial, geometric, and resilience parameters of the test engine and its mounts. These parameters and cycle-averaged combustion pressure measurements from the test engine are the inputs for the FCM. Model-experiment comparisons are made for steady-state engine operations, i.e., after the start-up transients in the test engine and model engine have subsided.

As might be expected, static and dynamic imbalance of the various rotating engine components (crankshaft and flywheel) and mismatch between the primarily reciprocating ones (pistons and connecting rods) can lead to significant vibratory forcing of the engine block at the low engine orders. For a variety of reasons, the resulting engine vibrations are hard to predict in detail. Here, the precise imbalance and mismatch configuration of the test engine was unknown and essentially unobtainable. In addition, the FCM as currently formulated does not include every moving engine

[1]nee Winton. Currently at Ford Motor Company.

Contributed by the Internal Combustion Engine Division of THE AMERICAN SOCIETY OF MECHANICAL ENGINEERS for publication in the ASME JOURNAL OF ENGINEERING FOR GAS TURBINES AND POWER. Manuscript received by the ICE Division July 2000; final revision received by the ASME Headquarters Jan. 2001. Editor: D. N. Assanis.

component. In particular, the front-end gear train, overhead camshaft, and fuel delivery system were not included. Zhao and Reinhart [9] have shown that the gear train and the fuel delivery system are the dominant cause of engine noise at frequencies above a few hundred Hertz. Hence, the hope here is that the dynamics and vibration contributions of these components are small enough to neglect compared to the contributions from the modeled components. Thus, the final model-experiment comparisons presented in this paper are between a model engine having an incomplete set of moving internal components and plausible but hypothetical rotational imbalances and component mismatches, and the test engine having a complete set of moving internal components but unknown imbalances and mismatches.

The remainder of this paper is divided into four sections. The next one covers the experimental setup and the measurement techniques. Section 3 describes how the quiescent engine modal analysis was used to set parameters in the FCM engine vibration model. Section 4 presents comparisons between the model output and experimental engine for vibration loads transmitted to the engine mounting structure. The final section summarizes this effort and provides a few conclusions.

2 Experimental Measurements

The experimental setup has been described in Winton and Dowling [10] and Hoffman and Dowling [8], so the following summary is brief. The test engine was a four-stroke inline six-cylinder heavy-duty Diesel engine with a nominal (wet) weight of 13,000 N, displacement of 12.7 liters, rated power of 350 kW at 2100 rpm, and peak torque of 2100 N-m at 1200 rpm. The engine was loaded by an electric dynamometer and was operated at rated-speed and peak-torque speed for this study. Torque measurements were made with a calibrated strain-gauge load cell and are accurate to ± 2 percent. Engine speed was monitored by magnetically counting teeth on a 60-tooth gear attached to the engine's crankshaft. The engine was supported on three instrumented mounts incorporating elastomeric isolation elements and three-component strain-gauge load cells. The rear mounts each employed one isolator (Lord Corporation CB 2204-2) and one three-component 22,240 N (5,000 lbf) vertical capacity load cell (AMTI MC5-3-5000). The front mount employed two isolators (Lord Corp. SSB33-1000-4) and a three-component 44,480 N (10,000 lbf) vertical capacity load cell (AMTI MC5-4-1000). The use of isolators with this test engine (unlike the hard-mounting common in industrial engine tests) was intended to ensure that the results would be applicable to vehicle design. The nine load-cell outputs (three per mount) were amplified with AMTI signal conditioners, low pass filtered below 1.05 kHz, and 16-bit digitized at 2.1 kHz for 5 seconds using Tektronix data acquisition hardware, LABVIEW™ software (from National Instruments), and a PC-type computer.

Experimental data was acquired in three steps. First, the warmed-up but quiescent engine was subjected to standard impact hammer modal analysis with output force measurements replacing the usual accelerometer or proximity probe measurements. The measured-force time-series data were Fourier analyzed and then curve-fit using commercial software (the STAR system from Spectral Dynamics, Inc.) to determine the modal frequencies, modal dampings, and modal force signatures for the six lowest-frequency modes. The six lowest modal frequencies were found to lie between 5.6 and 26.3 Hz and were assumed to describe the quiescent rigid-body modes of the mounted engine. As described in the next section, these measurements were used to optimize inertial, geometrical, and mount resilience parameters for use in the FCM.

For the second step, data was collected while the test engine was run at two extreme operating points, full load at peak torque speed (1200 rpm, 2061 N-m) and full load at rated speed (2100 rpm, 1654 N-m). These operating points were chosen since they generally represent the extreme vibration cases for this engine and thereby provide a stringent test of the rigid-body-based FCM. Thus, the results presented for the success of the model in Section IV are conservative. Because of experiment-specific limitations associated with the engine's mounting system, vibration frequencies above 200 Hz are not reported because of contamination vibration of the engine's mounting structure.

The final step of the data acquisition involved measurement of the in-cylinder combustion pressures while the engine was running. Here, a special engine cylinder head modified to accept at least one pressure sensor in each cylinder was used to make simultaneous in-cylinder pressure measurements in all six cylinders while the engine was running at steady-state at the two test conditions. The temporal resolution of these measurements was 1/4 of a crank angle degree and data was collected for 86 engine cycles. The final temporal pressure profiles used in the FCM were cycle-averaged measurements.

Unfortunately, the cylinder pressure measurements and the vibratory force measurements both required the full resources of the available data acquisition system so the two types of measurements could not be obtained simultaneously. Because of this limitation, the in-cylinder pressure measurements were made after the vibration measurements and minor (two percent to four percent) adjustments were made to the cycle-averaged pressure measurements to account for the day-to-day variations in engine performance. A time-based trigger was used in vibration data acquisition instead of a crankshaft angle-based trigger for simplicity.

3 Quiescent-Engine Model-Experiment Matching

Some of the parameters needed from the fully instrumented ready-to-run test engine for use in the FCM were either unknown or known with only limited certainty. Such parameters included the components of the engine's moment of inertia, the three-dimensional location of the engine's center of mass, and the engine-mount isolator stiffnesses and dampings. To refine the values of these parameters, modal-analysis measurements were combined with the multi-objective goal attainment capability found in MATLAB®. The procedure was as follows. A set of original estimates for these parameters was produced by the simple calculations, simple measurements, reference to manufacturer's data sheets, or educated guesses. An objective function was formulated that included predicted and experimentally determined modal frequencies, modal dampings, and selected components of the modal force signatures for the six lowest-frequency modes of the quiescent test engine. Limits were then set on the parametric space available for the optimization, and the MATLAB® optimizer was put to work to match the measured modal parameters by adjusting the estimated parameter values to minimize the objective function. Weight factors within the objective function were chosen so that greater emphasis was put on matching modal frequencies compared to modal dampings. The modal analysis optimization was completed for one reference position of the piston-rod-crankshaft system (piston no. 1 at top dead center). Because of the symmetry of the inline six-cylinder configuration and the approximate nature of the optimization, it was not necessary to adjust the experimental engine to the same configuration for the experimental modal analysis.

In principle this modal matching approach is simple but in order to allow the optimizer to attain a solution in a reasonable amount of time, the objective function had to be simplified. This was accomplished in three ways. First, the optimizer was allowed to seek a solution for the engine's inertial parameters without considering damping. This meant that the experimentally measured modal-analysis force signatures had to be projected on to the real axis, e.g., the relative phase of the various modal force signature components was accounted for by positive or negative signs alone. Fortunately, this approximation is acceptable because the measured modal dampings are small (typically less than seven percent of critical damping), and the phases of the components of the modal force signatures are typically close to either 0 deg or 180 deg. Second, only the largest modal signature components for

Table 1 Nonoptimized and optimized moment of inertial (*I*) and center of mass (*a*) parameters for the engine with respect to a reference point that lies at the intersection of the crankshaft axis and the centerline of the cylinder closest to the front of the engine

Engine block parameter	Original numerical value	Optimized numerical value
I_{xx}	214 kg-m^2	256 kg-m^2
I_{yy}	484 kg-m^2	671 kg-m^2
I_{zz}	329 kg-m^2	521 kg-m^2
I_{xy}	0 kg-m^2	42.3 kg-m^2
I_{xz}	0 kg-m^2	-60.4 kg-m^2
I_{yz}	0 kg-m^2	56.7 kg-m^2
a_x	42.2 cm	44.3 cm
a_y	2.0 cm	-8.8 mm
a_z	27.5 cm	28.3 cm

each modal force signature were used in the optimization. And third, the matching of modal dampings was conducted after the engine's inertial parameters were set. The precise implementation details and parametric optimization ranges are provided in Hoffmann [7]. The results of this optimization procedure are given in Tables 1 and 2 that list the original nonoptimized and final optimized values for the engine-inertial and mount-isolator parameters. These individual mount-isolator properties were then implemented into the model using the symmetrical matrix development presented in Part I.

The match obtained with the experimental engine is acceptable or even good. Tables 3 and 4 show a comparison of results for the optimized and experimental modal frequencies and dampings. Here the root-mean-square (RMS) fractional error is given by

$$\text{rms fractional error in } Y = \left[\frac{\Sigma_{i=1}^{6} (Y_{i,\text{exp}} - Y_{i,\text{opt}})^2}{\Sigma_{i=1}^{6} (Y_{i,\text{exp}})^2} \right]^{1/2} \quad (1)$$

where Y is the parameter of interest (frequency, damping, etc.), the subscript ''i'' refers to the mode number, the subscript ''exp'' refers to an experimental measurement, and the subscript ''opt'' refers to an optimized value. A comparison of the measured and optimized nine-component modal force signatures for the six lowest-frequency modes is omitted for brevity; however, the rms errors, when defined similarly to (1), between the measured and optimized modal signatures varied between 0.16 and 0.30. Although larger than the errors on the modal frequencies or dampings, these modal force signature errors are acceptable because they lie near the repeatability accuracy of the experimental modal analysis.

Table 3 Computed and measured quiescent-engine modal frequencies

Mode	Optimized modal frequency (Hz)	Experimental modal frequency (Hz)
1	5.85	5.68
2	9.48	9.76
3	12.47	12.84
4	13.38	13.53
5	21.59	20.98
6	26.01	26.25
	0.021 RMS Error	

Table 4 Computed and measured quiescent-engine modal dampings

Mode	Optimized modal damping (Hz)	Experimental modal damping (Hz)
1	0.3106	0.37644
2	0.4729	0.53009
3	0.7921	0.67417
4	0.4910	0.59505
5	0.6258	0.72919
6	0.7569	0.91734
	0.16 RMS Error	

Table 2 Nonoptimized and optimized engine mount stiffnesses (*k*) and dampings (*c*)

	Stiffness	Original value	Optimized value	Damping	Original value	Optimized value
Left rear	k_x	$1.88 \times 10^6 \frac{N}{m}$	$2.08 \times 10^6 \frac{N}{m}$	c_x	$2990 \frac{N \cdot s}{m}$	$842 \frac{N \cdot s}{m}$
	k_y	same as above	same as above	c_y	same as above	same as above
	k_z	$9.42 \times 10^5 \frac{N}{m}$	$1.86 \times 10^6 \frac{N}{m}$	c_z	$2110 \frac{N \cdot s}{m}$	$6878 \frac{N \cdot s}{m}$
Right rear	k_x	$1.88 \times 10^6 \frac{N}{m}$	$1.96 \times 10^6 \frac{N}{m}$	c_x	same as original left rear c_x	same as optimized left rear c_x
	k_y	same as above	same as above	c_y	same as original left rear c_x	same as optimized left rear c_x
	k_z	$9.42 \times 10^5 \frac{N}{m}$	$2.13 \times 10^6 \frac{N}{m}$	c_z	same as original left rear c_z	same as optimized left rear c_z
Front	k_x	$1.16 \times 10^6 \frac{N}{m}$	$3.22 \times 10^6 \frac{N}{m}$	c_x	$2340 \frac{N \cdot s}{m}$	$0 \frac{N \cdot s}{m}$
	k_y	same as above	same as above	c_y	same as above	same as above
	k_z	$8.48 \times 10^6 \frac{N}{m}$	$12.1 \times 10^6 \frac{N}{m}$	c_z	$6340 \frac{N \cdot s}{m}$	$3652 \frac{N \cdot s}{m}$

Overall, even though the search space for the optimizer was quite large, all the parameters were viable for the test engine. The final optimized parameters are not necessarily unique; however, as this study shows, uniqueness is not essential due to the model's robustness to variations in modal parameters. Thus, the vibration characteristics of the model and experimental quiescent engines were matched.

4 Running Engine Comparisons

This section presents a comparison of the FCM output with experimental measurements. The OWCM presented in Part I [6] is not included here because, as found in Part I, the OWCM and the FCM produce similar results for the well-balanced, inline six-cylinder engine (± 5 percent or smaller differences). There are really two challenges in predicting the vibratory behavior of the experimental engine. First, the geometrical and inertial parameters of the engine, and the geometry, stiffness, and damping of the engine's mounting system must be identified. This was accomplished through the procedure described in Section 3. The second challenge is to determine: (i) the actual variations in the test engine's internal components, (ii) the static and dynamic imbalance of the assembled crankshaft-flywheel system within the test engine, and (iii) the dynamic and vibratory effects of the unmodeled engine components. As described in Part I, small inertial mismatches between components and any static or dynamic imbalances can dramatically change the vibration response of the running engine. Unfortunately, the resources did not exist to disassemble the test engine and identify the various imperfections at a component level so the unique mismatches and imbalances of the test engine were unknown. In addition, the FCM does not include every moving component. Thus, the comparisons provided here are drawn between a model engine with a hypothetical set of imperfections and an incomplete set of moving internal components, and the test engine with an actual set of imperfections and a complete set of moving internal components.

The process for finding appropriate hypothetical component mismatches and imbalances began with a baseline model prediction for an engine lacking any imperfections. The baseline-model vibration amplitudes were up to an order of magnitude below the measured vibration levels. A short slate of engine component parameters were then varied by trial and error within the FCM to enhance the predicted vibration levels and better match the model to the experiment. (Use of optimization routines for this task exceeded the capacity of the available computational resources.) The component parameters varied were the size and location of two crankshaft imbalance masses and the six piston masses. Although a much larger number of components and component parameters exist in the six-cylinder piston-rod-crankshaft mechanism, the parameters selected for trial and error adjustments provided more than enough parameter space in which to attempt the experiment-model matching. Table 5 lists the final adjustments made to the baseline component parameter values. It must be noted here that the selections shown in Table 5 are the results of an incomplete search of the available parameter space and that many other parameter combinations might yield similar (or even superior) results. Although the piston-weight mismatches and imbalance levels may seem too large on an individual basis, they effectively represent the overall inertial mismatch and imbalance level of all the engine's components. Hence, although they are almost surely fictitious, these selected imperfections are not necessarily unreasonable.

The comparisons made here are for the three-component vibration forces transmitted through the elastomeric isolation elements to the engine's supporting structure at the engine's three mounts. The model is driven with the measured (and adjusted) average pressure time-histories for each cylinder. The parameter modifications listed in Table 5 were used to bring the vibration level of the model engine close to the vibration level of the test engine. Both the optimized and nonoptimized engine and mount parameters (see Tables 1 and 2) were used in the model. Two additional adjustments were made to match the FCM and the experiment. First, the load torque used in the model was five to six percent larger than the measurements to account for engine friction. This adjustment causes the model engine to rotate at the same speed as the test engine. Second, because the engine mount forces were measured without an absolute crank angle reference, the model output is shifted in time with respect to the experimental measurements to provide the best matchup between the two types of results.

Figures 1 and 2 show the spectral force magnitudes of the measured and predicted engine mount forces for optimized engine and mount parameters. Figure 1 shows the full load at peak torque speed results, and Fig. 2 shows the full load at rated speed results. Both figures display nine panels in a three-by-three array. Each row of panels comes from the same engine mount. Each column of panels provides force spectra from the same Cartesian direction (x, y, or z). Here the x-direction points from the front to the rear of the engine, the y-direction points out the right side of the engine when the engine is viewed from behind, and the z-direction points vertically upward (opposite gravity). The $\times$'s in each figure denote the predicted spectral amplitude at half and whole engine orders. The solid lines are the experimental spectra.

Although the comparisons shown on Figs. 1 and 2 are far from perfect, the overall trends are captured well. The largest vibration

Table 5 Parameter modifications used in the fully coupled model (FCM) to match the experiment. The piston mass number represent the percentage change in each piston. The numbers for the crankshaft imbalances are: the point mass sizes, their radial distance from the crankshaft axis of rotation, their *x*-locaiton along the crankshaft axis from the reference point (intersection the axis of cylinder No. one with the crankshaft axis), and the angular displacement when piston no. one is at top dead center.

Piston Masses	Crankshaft Imbalance
#1 –> +2.5%	Point Mass No. 1.
#2 –> +2.5%	mass = 1 kg, radius = 5.0 mm, axial distance = -0.282 m, angle = +120°
#3 –> no change	
#4 –> no change	Point Mass No. 2.
#5 –> -2.5%	mass = 1 kg, radius = 6.5 mm, axial distance = 1.006 m, angle = 0°
#6 –> -2.5%	

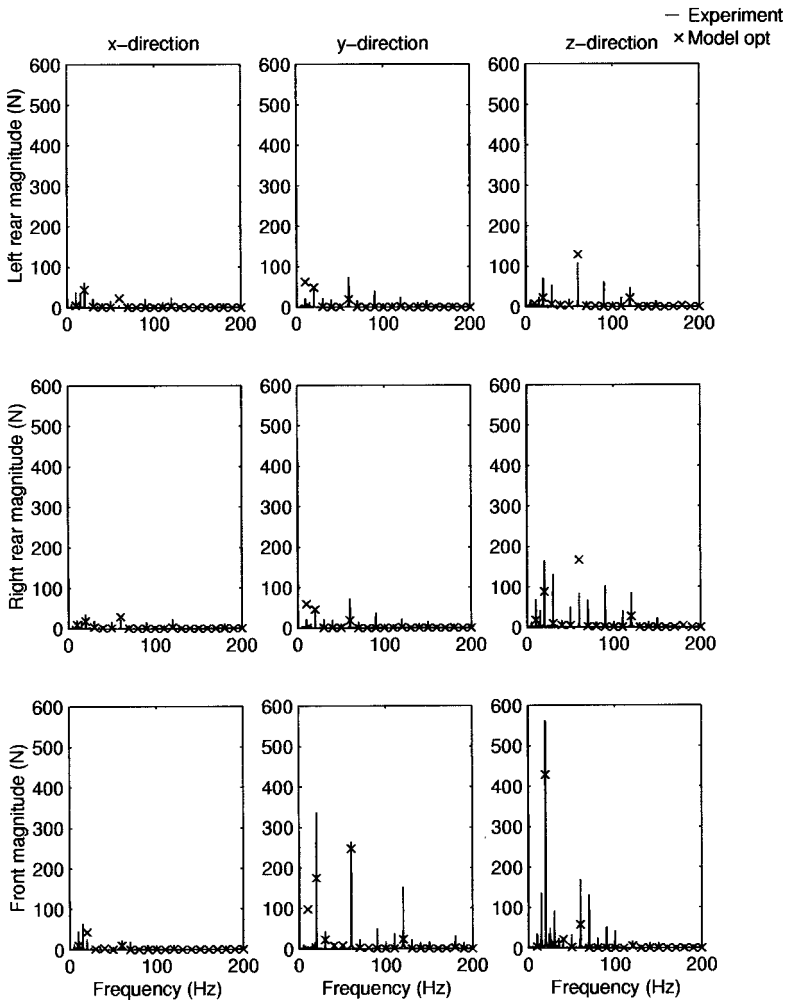

Fig. 1 Measured and simulated engine mount force magnitudes versus frequency for an in-line six-cylinder heavy-duty Diesel engine running at a speed of 1200 rpm with a load torque of 2061 N-m. The simulated engine used the optimized parameters given in Tables 1 and 2 and component imperfections listed in Table 5. The solid line denotes the experimental data. The ×'s denote the simulation results at half and whole engine orders.

forces are predicted to occur in the vertical direction on all mounts and in the *y*-direction (side-to-side) on the front mount. Comparatively smaller vibration forces are expected in the *x*-direction (front-to-back) on all mounts and in the *y*-direction on the rear mounts. The experimental results on Figs. 1 and 2 both follow these trends. All plot vertical axes were constrained to be the same to facilitate component/mount force comparisons. In addition, the FCM only predicts engine vibration at the half, first, second, third, and sixth engine orders while the engine actually vibrates at a greater range of frequencies. First order is the most important engine vibration frequency at both speeds and the match between the model and experiment is reasonable. An appropriate extension of (1) produces an rms fractional error (averaged across mounts and directions) for the model of 0.33 and 0.35 at first order for the peak-torque speed and rated speed results, respectively. At third order, the rms fractional error is larger 0.45 and 0.72 for the peak-torque speed and rated speed results, respectively. These larger third-order differences can be attributed to the high-amplitude cyclic torques exerted on the crankshaft and the engine block by the camshaft-driven fuel-injection system which fires three times per engine rotation, but was not included in the FCM.

There are also important differences between the results from the model and the experiment. The FCM does not adequately predict any of the experimentally measured higher half-order vibration frequencies (e.g., engine orders 3/2, 5/2, 7/2, 9/2, etc.). The engine's response at these frequencies may be nonrigid and therefore beyond the model's capability. This contention is supported by the findings of Nakada [11] and Reinhart [12] who attribute higher half-order vibrations to flexible engine motions.

The comparisons provided on Figs. 1 and 2 can also be cast into the time domain where the temporal phasing of the predicted engine vibration response at the various engine orders is readily apparent. Such comparisons are provided on Figs. 3 and 4, which slow the predicted and measured force-time histories covering two crankshaft rotations at peak-torque and rated speeds, respectively. Here, both the experimental and computational results have been low-pass filtered to include frequencies at third engine order and below. As for Figs. 1 and 2, the three-by-three array of panels in Figs. 3 and 4 are arrayed so that rows correspond to the same engine mount and columns correspond to the same Cartesian direction. The dark solid lines are the experimental measurements. The light solid lines are the FCM results with optimized parameters. The dashed lines are the FCM results with nonoptimized parameters. Again, the overall predictions are good with large

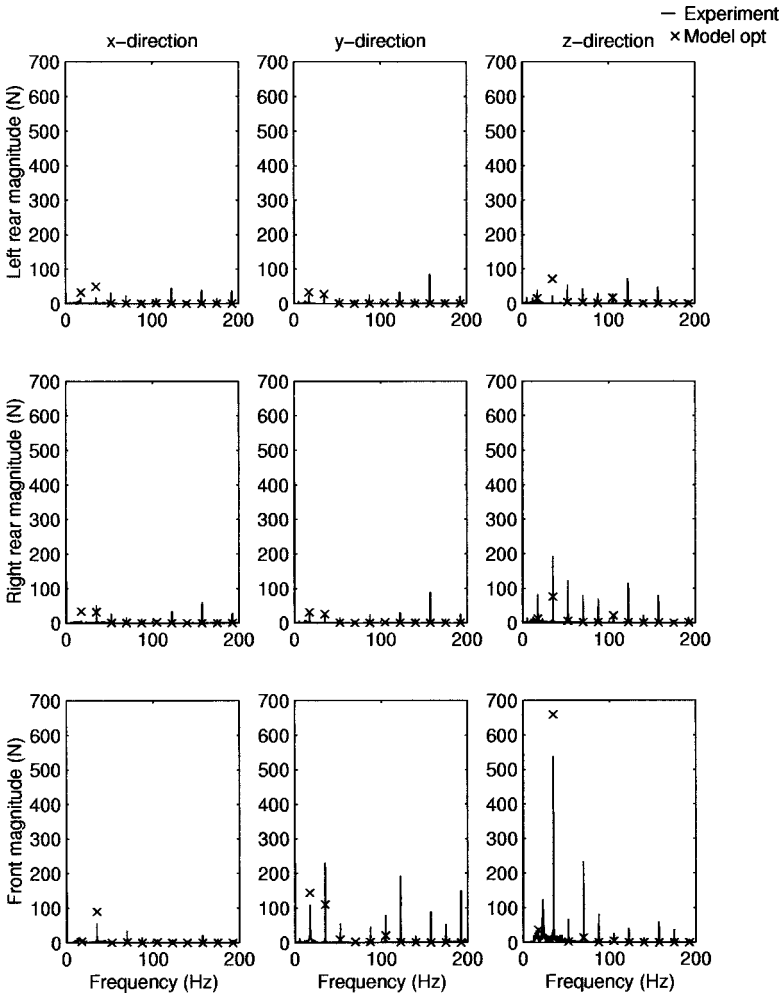

Fig. 2 Same as Fig. 1 except the engine is running at a speed of 2100 rpm with a load torque of 1640 N-m

(small) simulated vibration forces occurring where large (small) forces were measured. The most apparent mismatch between the model and the experiment (more easily seen in Fig. 4) can be traced to the amplitude and phasing of the third-order oscillations. Again, this discrepancy is most likely due to unmodeled third-order cyclic torques that are applied to the crankshaft and engine block by the engine's gear train and overhead camshaft in order to drive the engine's unit fuel injectors.

The results shown on Figs. 1–4 can be summarized by the overall model-experiment correlation coefficient, C:

$$C=\frac{\Sigma_{i=1}^{3}\Sigma_{j=1}^{3}(1/\tau)\int_0^\tau F_{m,ij}(t)F_{p,ij}(t)dt}{[\Sigma_{i=1}^{3}\Sigma_{j=1}^{3}(1/\tau)\int_0^\tau F_{m,ij}^2 dt]^{1/2}[\Sigma_{i=1}^{3}\Sigma_{j=1}^{3}(1/\tau)\int_0^\tau F_{p,ij}^2 dt]^{1/2}}, \quad (2)$$

where i is the direction number, j is the mount number, $F_{m,ij}$ is the measured engine mount force in direction i on mount j, and $F_{p,ij}$ is the FCM predicted mount force in direction i on mount j, and τ corresponds to seven complete engine cycles. Table 6 provides values of C for both operating points, for optimized and nonoptimized engine parameters, and for bandwidths up to 200 Hz and up through third engine order. The purpose of this correlation effort was to evaluate the overall performance of the model with a particular emphasis on matching the dominant mount forces. A detailed comparison of the individual mount and direction correlation coefficients is deferred until a more complete engine model (that includes the camshaft and front-end gear train, for example) is readied. As expected, the correlation coefficients for the more restrictive bandwidths (third engine order and below) are higher because the FCM does not predict as much high-frequency vibration as the test engine produces. However, all the values in Table 6 are above +0.50, which indicates that model and the experiment are in general agreement. Interestingly, the optimized parameters do not produce superior correlation values under both operating conditions. This suggests that the modeling approach embodied by the FCM is robust enough to predict engine mount forces with better than 0.50 correlation even when some important engine block geometrical and inertial parameters are approximations of the actual engine parameters. Hence detailed parameter identification is possibly unnecessary for use of the FCM, a valuable trait in preliminary design.

5 Summary and Conclusions

The key contribution here is the presentation of a comparison of the computational results from a seven degree-of-freedom fully coupled model of engine dynamics and vibration to experimental results obtained from three-component force measurements made at the three main mounts of a running inline six-cylinder heavy-duty Diesel engine. Estimated or poorly known engine parameters were determined through an optimization procedure for the vibration modes of the computational and experimental quiescent engines. Comparisons of the predicted and measured mount forces are presented in both the time and frequency domains with guarded success.

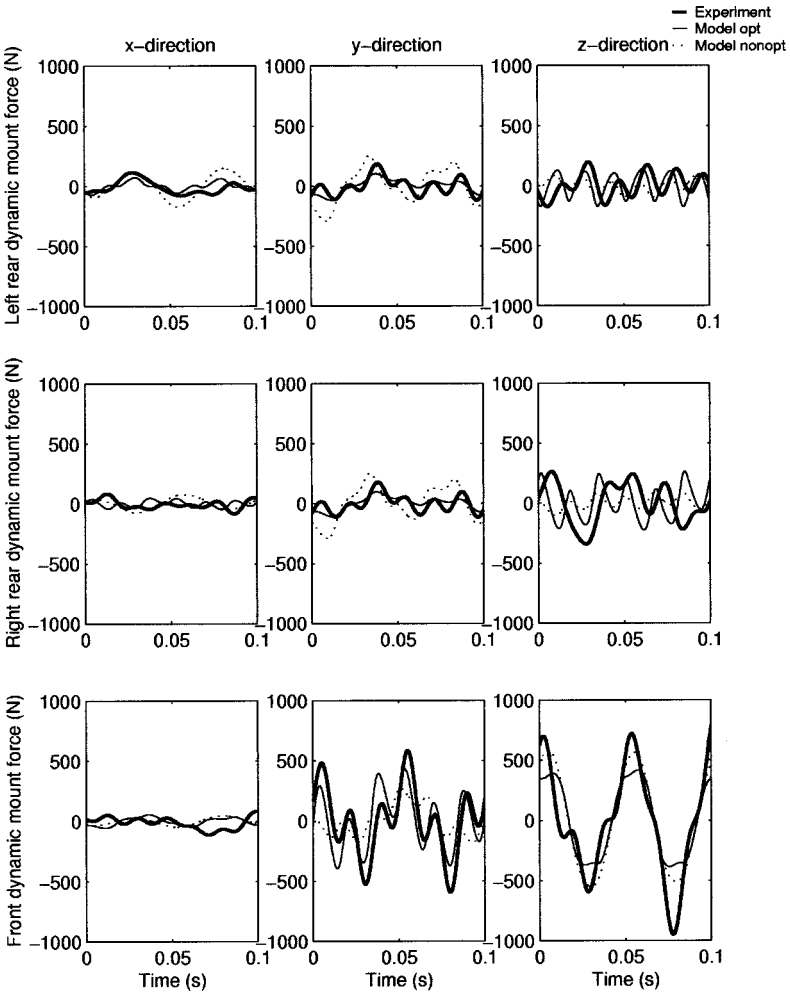

Fig. 3 Measured and simulated engine mount forces versus time for an in-line six-cylinder heavy-duty Diesel engine running at a speed of 1200 rpm with a load torque of 2061 N-m. The heavy solid line is the experimental data. The light solid line is the simulated engine with the optimized parameters given in Tables 1 and 2. The dotted line is the simulated engine with the nonoptimized parameters given in Tables 1 and 2. Both simulations use the component imperfections listed in Table 5. All three data sets are low-pass filtered to include only vibration frequencies up to third engine order and the time duration shown corresponds to two engine rotations (720 crankangle degrees).

The results presented here support three conclusions. First, the new engine model described in our companion paper (Part I) is able to provide adequate, but imperfect, predictions of engine vibrations in the frequency range where rigid-body motions of the engine block and its internal components dominate. Vibration force levels were simulated correctly for the various mounts in the various directions. Current model-experiment correlation coefficients are as high as 0.70 and do not fall below 0.50. These correlation values are actually better than they first appear; a model-experiment correlation coefficient of 1.0 is impossible for a rigid-body model because of nonrigid engine components (oil, coolant) and flexible engine motions. In fact, only 85 to 90 percent of the test engine's vibratory motion can be accounted for by rigid-body modes under the test conditions considered here ([8]). Thus, the correlation coefficients found here suggest that the fully coupled model compares favorably to experimental force measurements within the limits imposed by rigid-body modeling. Moreover, the vibration contribution of engine components and systems that were not modeled may explain much of the remaining model-experiment differences.

Second, precise knowledge of an engine's inertial and geometrical parameters, and its mount isolator stiffnesses and dampings is not necessary to obtain acceptable predictions from the fully coupled model. This is a major advantage for preliminary design work when many parameter values may only be known approximately or may be based on historical or benchmark information.

And finally, moving internal-component mismatches and static and rotating imbalances are the most important source of vibration for engines whose configurations are naturally well balanced. In the present study, the computationally perfect inline six-cylinder engine produces vibration levels that are at least an order of magnitude below the measured vibration levels for a nominally identical test engine. Thus, use of a model like the FCM by engine designers could lead to better tolerancing for the inertial and geometrical parameters of moving internal engine components. For example, precise matching of piston masses may not be necessary if the connecting rods cannot be matched to a similarly stringent tolerance.

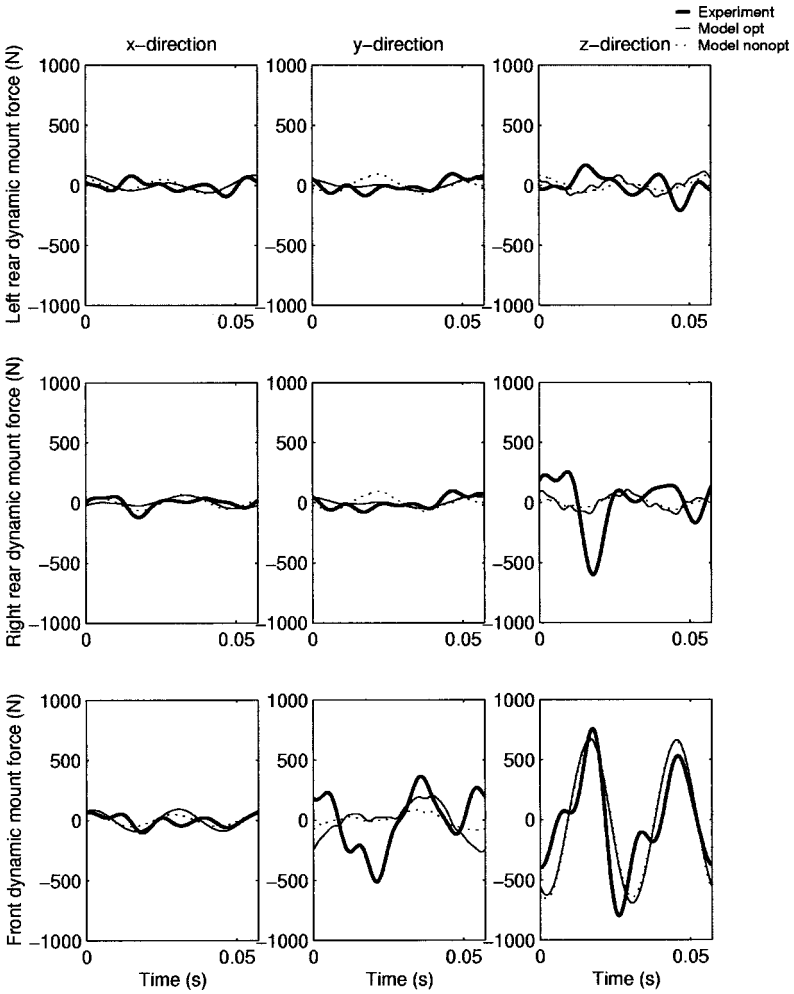

Fig. 4 Same as Fig. 3 except the engine is running at a speed of 2100 rpm with a load torque of 1640 N-m

Table 6 Overall model-experiment correlation coefficients for mount force time-histories low-pass filtered at 200 Hz and third engine order for an inline six-cylinder heavy-duty Diesel engine running at a full load at speeds of 1200 and 2100 rpm using optimized and nonoptimized parameters

		Corr. Coeff.	
Speed	Parameters	≤ 200 Hz	≤ 3rd order
1200 rpm	optimized	0.65	0.70
	non-optimized	0.58	0.63
2100 rpm	optimized	0.52	0.58
	non-optimized	0.57	0.65

Acknowledgments

The in-cylinder pressure measurements were provided to the authors by Samuel Homsy and Scott Fiveland who were conducting a concurrent thermodynamic performance study of the test engine. This research project was supported by Cummins Engine Company, Inc. and the U.S. Army Tank Automotive Research, Development and Engineering Center (TARDEC) through the Automotive Research Center (Contract No. DAAE07-94-C-R094) at the University of Michigan.

References

[1] Norling, R. L., 1978, ''Continuous Time Simulation of Forces and Motion Within an Automotive Engine,'' SAE paper No. 780665.
[2] Shiao, Y.-J., Pan, C.-H., and Moskwa, J. J., 1994, ''Advanced Dynamic Spark Ignition Engine Modeling for Diagnostics and Control,'' Int. J. Veh. Des., **15**, pp. 578–596.
[3] Snyman, J. A., Heyns, P. S., and Vermeulen, P. J., 1995, ''Vibration Isolation of a Mounted Engine Through Optimization,'' Mech. Mach. Theory, **30**, pp. 109–118.
[4] Suh, C.-H., and Smith, C. G., 1997, ''Dynamic Simulation of Engine-Mount Systems,'' SAE paper No. 971940.
[5] Hoffman, D. M. W., and Dowling, D. R., 1999, ''Modeling Fully Coupled Rigid Engine Dynamics and Vibrations,'' SAE Paper No. 1999-01-1749, *Proceedings, 1999 SAE Noise and Vibrations Conference*, Vol. 2, Traverse City, MI, Society of Automotive Engineers, Warrendale, PA, pp. 747–755.
[6] Hoffman, D. M. W., and Dowling, D. R., 2001, ''Fully Coupled Rigid Engine Dynamics and Vibrations—Part I: Model Description,'' ASME J. Eng. Gas Turbines Power, **123**, pp. 677–684.
[7] Hoffman, D. M. W., 1999, ''In-Line Internal Combustion Engine Dynamics and Vibration,'' Ph.D. thesis, University of Michigan, Ann Arbor, MI.
[8] Hoffman, D. M. W., and Dowling, D. R., 1999, ''Limitations of Rigid Body Descriptions for Heavy-Duty Diesel Engine Vibration,'' ASME J. Eng. Gas Turbines Power, **121**, pp. 197–204.
[9] Zhao, H., and Reinhart, T., 1999, ''The Influence of Diesel Engine Architecture on Noise Levels,'' SAE Paper No. 1999-01-1747, *Proceedings, 1999 SAE Noise and Vibrations Conference*, Vol. 2, Traverse City, MI, Society of Automotive Engineers, Warrendale, PA, pp. 729–735.
[10] Winton (Hoffman), D. M., and Dowling, D. R., 1997, ''Modal Content of Heavy-Duty Diesel Engine Block Vibration,'' SAE Trans., **106**, Section 6, Part 2, pp. 2802–2811 (SAE Paper No. 971948).
[11] Nakada, T., and Tonosaki, H., 1994, ''Study of the Excitation Mechanism of Half-Order Vibrations in an In-Line 4-Cylinder Internal Combustion Engine,'' Trans. Jpn. Soc. Mech. Eng., Ser. C, **60**, No. 577, pp. 2977–2983.
[12] Reinhart, T. E., 1997, private communication, Cummins Engine Company, Inc., Columbus, IN.